Central East Pacific Flight Routing

Shon Grabbe*, Banavar Sridhar†, and Parimal Kopardekar‡
NASA Ames Research Center, Moffett Field, CA, 94035-1000

Nadia Cheng§
University of California—San Diego, La Jolla, CA, 92093-0411

With the introduction of the Federal Aviation Administration's Advanced Technology and Oceanic Procedures system at the Oakland Oceanic Center, a level of automation now exists in the oceanic environment to potentially begin accommodating increased user preferred routing requests. This paper presents the results of an initial feasibility assessment which examines the potential benefits of transitioning from the fixed Central East Pacific routes to user preferred routes. As a surrogate for the actual user-provided routing requests, a minimum-travel-time, wind-optimal dynamic programming algorithm was developed and utilized in this paper. After first describing the characteristics (e.g., origin airport, destination airport, vertical distribution and temporal distribution) of the westbound flights utilizing the Central East Pacific routes on Dec. 14-16 and 19-20, the results of both a flight-plan-based simulation and a wind-optimal-based simulation are presented. Whereas the lateral and longitudinal distribution of the aircraft trajectories in these two simulations varied dramatically, the number of simulated first-loss-of-separation events remained relatively constant. One area of concern that was uncovered in this initial analysis was a potential workload issue associated with the redistribution of traffic in the oceanic sectors due to the prevailing wind patterns.

I. Introduction

The Oakland Oceanic Flight Information Region (FIR) (or Center), which is shown in Fig. 1, controls approximately 21.3 million square miles of airspace and borders the Anchorage FIR to the North, the Tokyo FIR to the East, the Aukland FIR to the South, and the coastline of the contiguous United States on the West[1]. In contrast, the twenty Air Route Traffic Control Centers (ARTCCs) in the contiguous U.S. encompass roughly 3 million square miles. Despite the vast amount of airspace controlled by this Center, flights, for the most part, are required to fly along fixed route structures and adhere to lateral separation standards that extend up to 100 nmi, longitudinal separation standards extending up to 15 minutes, and vertical separation standards of 1000 ft [2]. These stringent separation standards are required because of the limited surveillance capabilities in the ocean and the FAA's legacy Oceanic Display and Planning System (ODAPS). It is worth noting that both the lateral and longitudinal separation standards can be significantly reduced for Automatic Dependent Surveillance – Contract (ADS-C) equipped flights that are operating in regions of the Pacific that are designated for Required Navigation Performance (RNP) [2].

* Research Scientist, Automation Concepts Research Branch, Mail Stop 210-10, E-mail: Shon.R.Grabbe@nasa.gov.
† Chief, Automation Concepts Research Branch, Mail Stop 210-10, Fellow AIAA
‡ Project Manager, Advanced Air Transportation Technologies Office, Mail Stop 210-15
§ Student, Dept. of Mechanical and Aerospace Engineering

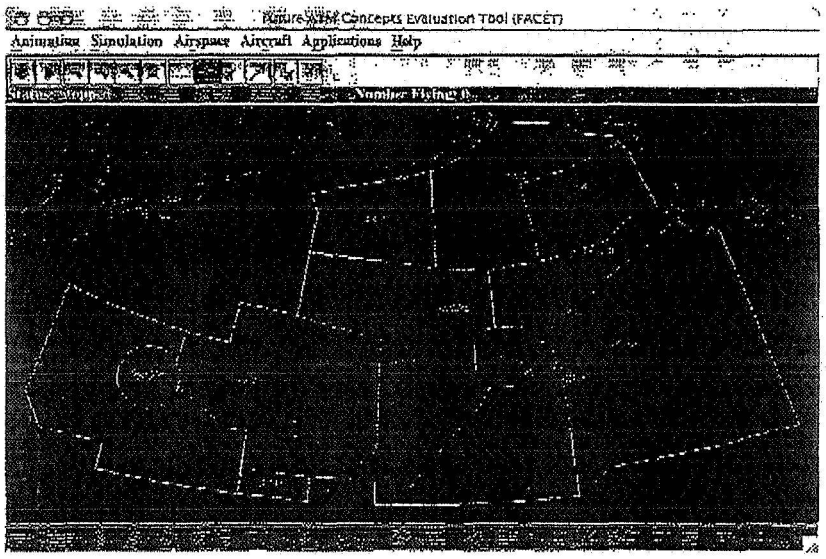

Figure 1. Oakland Oceanic Center Display Including Sector Boundaries and Coastal Map

With the introduction of the FAA's new Advanced Technologies & Oceanic Procedures (ATOP) at Oakland Center in 2005, increased route flexibility and reduced separation standards can potentially now be accommodated. Some of the major ATOP innovations leading to this increased flexibility are (1) fully integrated flight- and radar-data-processing capabilities, (2) conflict-detection capabilities, and (3) satellite data-link communication and surveillance capabilities [3]. This paper presents the results of an initial study, which examines the potential benefits and consequences of allowing user-preferred routing in place of the fixed Central East Pacific (CEP) routes.

The CEP routes shown in Fig. 2 connect the west coast of the United States to Hawaii. The alphanumeric designators for these seven routes are R463, R464, R465, R585, R576, and R577. Sectors OC-3 and OC-4 in the Oakland Oceanic FIR handles traffic along these routes. Routes R464 and R576 are used exclusively for westbound traffic, while routes R465, R585, and R577 are used exclusively for eastbound traffic. Routes R463 and R578 can accommodate bi-directional traffic. The RNP for aircraft flying on the CEP routes is 10, or RNP-10, which implies that the total horizontal position error of the aircraft cannot exceed 10 nmi for more than 95% of the flight time [2], [4]. These flights can be identified by the "/R" equipment suffix appearing in their International Civil Aviation Organization (ICAO) flight plans. [5]. Based on the required equipage level for flights operating on the CEP routes, the lateral separation standards are 50 nmi, the longitudinal separation standards vary between 5 and 10 minutes, and the vertical separation standards are 1000 ft.

To our knowledge, this is the first study designed to explore the benefits of transitioning from the fixed CEP-based route structure to a more flexible user-preferred routing structure. Though the flight routing application in this study is believed to be unique, the general area of flight plan routing and flight path design has a long history [6]. Recent advances in this area include the conflict-free, wind optimal routing work that was introduced in Ref. 7, the dynamic network flow rerouting approach introduced in Ref. 8, and the fleet assignment and routing approach introduced in Ref. 9. A comprehensive summary of many of the earliest flight routing techniques can be found in Ref. 10.

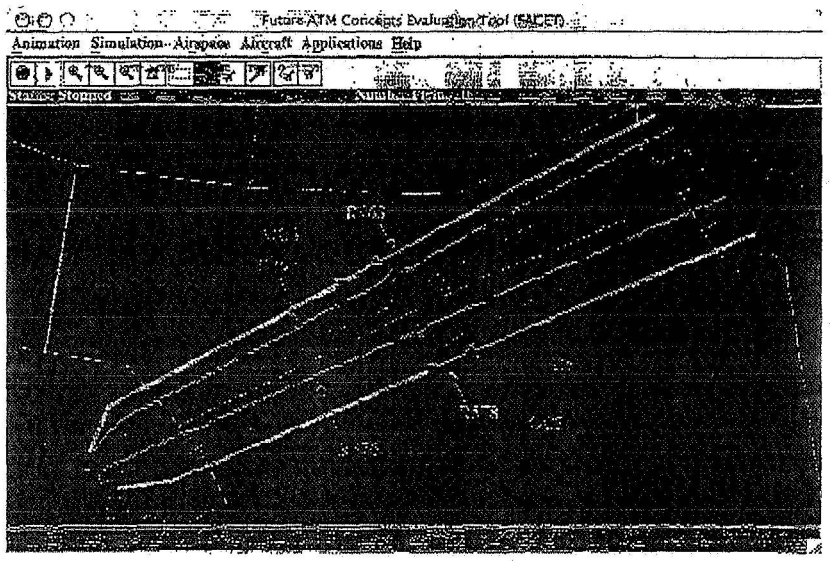

Figure 2. Central East Pacific (CEP) Routes

The rest of this paper is organized as follows. Section II describes the wind-optimal routing methodology that was adopted for this paper. The unmodified characteristics of the CEP routes are described in Section III and the modeling results are presented in Section IV. Finally Section V section ends with some conclusions.

II. Modeling Methodology

As previously mentioned, the FAA's new ATOP system offers an unprecedented level of automation in comparison to the legacy ODAPS system that it replaced. With this new system, it is now conceivable to transition from the fixed CEP route structure in the Pacific to a set of routes that accommodate the airline user's preferences. To begin understanding the potential implications of this transition, a minimum-travel-time, wind-optimal dynamic programming algorithm was developed to simulate possible user route preferences. Though the business models, schedules, and aerodynamic performance characteristics (e.g., engine type, weight, etc.) of the aircraft in the airline's fleet will ultimately govern the design of the optimal trajectories each airline wishes to fly, a simple minimum-time wind-optimal model, as adopted in this study, should initially suffice to understand this change in routing philosophy.

For the purpose of this study, the position of an aircraft along a minimum-time wind-optimal route at stage $k+1$ can be related to the position at stage k via the following equation:

$$x_{k+1} = x_k + u_k \tag{1}$$

Here u_k is the decision variable at stage k. For the purpose of this study, wind optimal routes are calculated on a grid composed of latitude and longitude values that encompass the region of airspace in which each analyzed aircraft travels. Though the grid is individually tailored for each flight, the grid is roughly bounded between the $20^{o}N$ latitude to the south, $40^{o}N$ latitude to the north, $156^{o}W$ longitude to the west, and $120^{o}W$ longitude to the east. This grid is sufficient for most flights that either depart or arrive at the west coast of the United States. For flights departing or arriving at in-land airports, such as Chicago O'Hare International Airport, the grid is increased accordingly.

The stages, k, within our problem formulation refer to the available longitudinal values; the states x_k refer to the latitude values; and the decision variables, u_k, are the changes in the latitude values that are permitted at each stage k. The bounds on the decision variables and the states are

$$\lambda_{\min,k} \leq x_k \leq \lambda_{\max,k} \tag{2}$$

$$u_k \in U_k \quad \text{where} \quad U_k = \{u_k | -5 \le u_k \le 5\} \tag{3}$$

Additional bounds are applied to x_k at the first and last stages to ensure the route starts and ends at the entry and exit points of the CEP routes into the Oakland Oceanic FIR. This additional constraint is applied to enforce any procedural constraints that might apply as an aircraft transitions to/from a U.S. Air Route Traffic Control Center (ARTCC) and the oceanic environment.

Using the principle of optimality, the minimum cost function at stage k, $I(x,k)$, can be calculated from the minimum cost function at stage $k+1$, $I(x_k + u_k, k+1)$ using the following expression [11]:

$$I(x,k) = \min_{u_k \in U_k} \{C(x_k, u_k, k) + I(x_k + u_k, k+1)\} \text{ for } k \in \{0,1,...,N-1\} \tag{4}$$

Here $C(x_k, u_k, k)$ is the cost associated with transitioning from state x_k to x_{k+1} using the decision variable u_k at stage k. For our study, the cost is equal to the amount of time required for an aircraft to fly from the current state, x_k, to the next state, x_{k+1}. The details of the cost function calculations are provided in Appendix A. The sequence of controls (i.e. $u_0, u_1, \ldots, u_{N-1}$) resulting from the solution of Eq. 5 for $0 \le k \le N-1$ is used to construct the minimum-time, wind-optimal routes between the origin and destination airport for each flight. For all routes generated using Eq. 4, the minimum cost function at $k=N$ (i.e. $I(x,N)$) has been set to zero.

To illustrate the use of this algorithm, wind optimal trajectories for the westbound aircraft that were nominally flying on the CEP routes are presented in the fourth section of this paper.

III. Unmodified Flow Characteristics

The primary purpose of this section is to describe the data sources used in this study and to familiarize the reader with the nominal characteristics (e.g., number of aircraft, vertical distribution, etc.) of the westbound traffic flying along the CEP routes. Aircraft flight plans, flight plan amendments, departure times, arrival times, and position reports were obtained from an Aircraft Situation Display to Industry (ASDI) data feed [12], [13] for Dec. 14-16 and 19-20 of 2005. For reference, Dec. 14th is a Wednesday and Dec. 20th is a Tuesday. To filter the westbound CEP route traffic from the national data mosaic provided by the ASDI data feed, only flights that explicitly contained R463, R464, R576, and R578 in either a flight plan or flight plan amendment message were retained for further processing. The resulting aircraft counts for this five-day period are shown in Fig. 3. A total of 325 westbound flights were analyzed during this time period. The average daily traffic count was 65 and the standard deviation was 4.6.

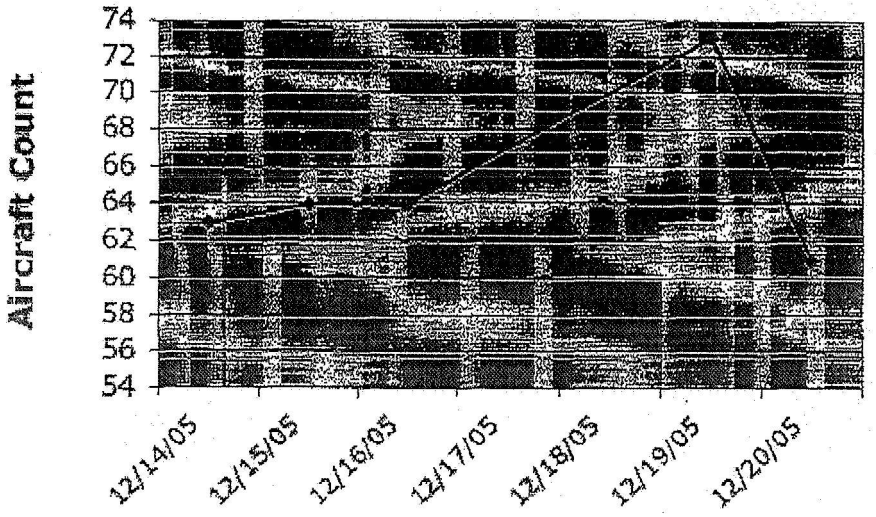

Figure 3. Westbound Traffic Counts on the CEP Routes

To assess the vertical distribution of the westbound flights, the actual flight level (FL) of each aircraft as it crossed 140° west longitude, which is roughly halfway between Hawaii and the U.S. mainland, was recorded and the results are displayed in the leftmost image in Fig. 4. As can be seen from this figure, the most predominantly used flight level was FL340 (or 34,000 ft), and approximately 73% of the aircraft were between FL320 and FL360.

The rightmost image in Fig. 4 depicts the temporal distribution of the westbound flights at 140° west longitude. As can be seen from this figure, the largest concentration of flights cross this longitude at roughly 19:00 UTC, which corresponds to a west-coast departure time of approximately 16:30 UTC (or 8:30 PST). The traffic count distribution on each of the analyzed days shows little variation, but slightly more aircraft were observed to cross this longitude at 6:00 UTC and 21:00 UTC on 12/19/05, which is a Monday.

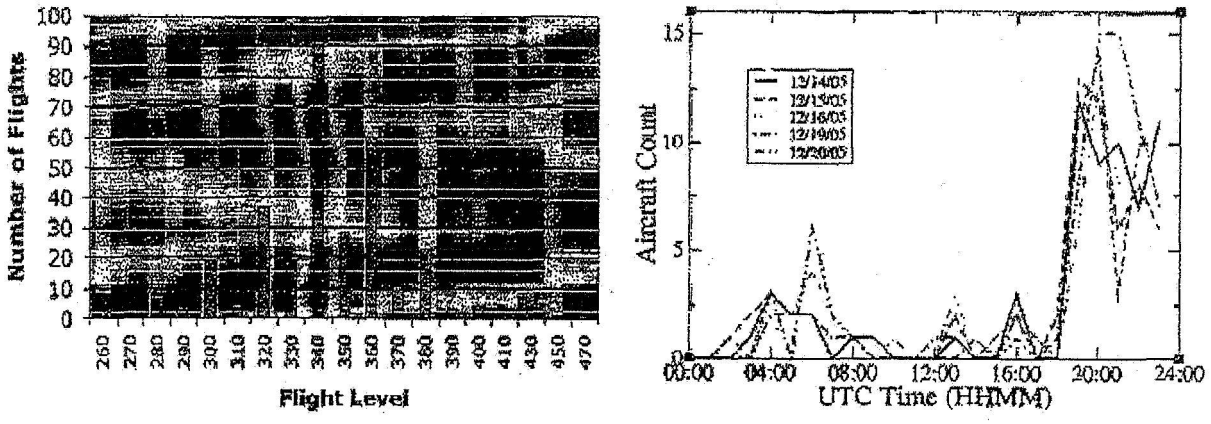

Figure 4. Vertical (left) and Temporal (right) Distribution of the West-Bound Flights at 140 degrees West Longitude

The leftmost image in Fig. 5 depicts the departure airport usage statistics for the westbound CEP flights, while the rightmost image shows the corresponding destination airport statistics. For the departure statistics, only the top 15 airports are illustrated, although flights were observed to depart from 40 airports during the five-day period

analyzed in this study. Roughly 42% of all westbound flights departed from Los Angeles International Airport, KLAX, and San Francisco International Airport, KSFO. The names associated with the remaining departure airport acronyms in Fig. 5 follow: Chicago O'Hare (KORD), McCarran Intl. (KLAS), Phoenix Sky Harbor Intl. (KPHX), John Wayne Airport (KSNA), Dallas/Fort Worth Intl. (KDFW), Metropolitan Oakland Intl. (KOAK), San Diego Intl. (KSAN), Memphis Intl. (KMEM), Ontario Intl. (KONT), Seattle-Tacoma Intl. (KSEA), Norman Y. Mineta San Jose Intl. (KSJC), Portland Intl. (KPDX), and Sacramento Intl. (KSMF).

The arrival airport statistics that are shown in the rightmost image in Fig. 5, illustrate that approximately 60% of all flights destined for Hawaii landed at Honolulu Intl. Airport (PHNL). In contrast, only one flight was observed to arrive at Lanai (PHNY) and Hilo (PHTO) during the same period. Of the remaining flights, 24% landed at Kahului (PHOG), 11% landed at Kona/Keahole Kailua (PHKO), and 4% landed at Lihue/Kauai Island (PHLI).

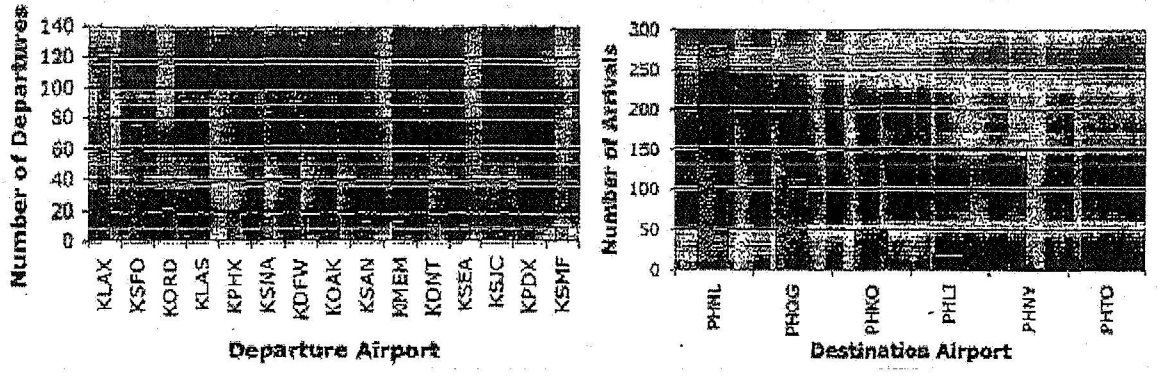

Figure 5. Top Origin and Destination Airports for the Westbound Flights

The distribution of the flights amongst the available westbound CEP routes is shown in Fig. 6. As shown by this figure, flights traveled predominately along R464 and R576, which are both undirectional routes. Significantly, less traffic was observed along R463 and R578, which are bi-directional routes. The control of flights along these routes was distributed roughly evenly between Oakland Oceanic Sectors 3 and 4. As illustrated by Fig. X, traffic on R463 and R464 is controlled by Sector 3, while traffic on R576 and R578 is controlled by Sector 4.

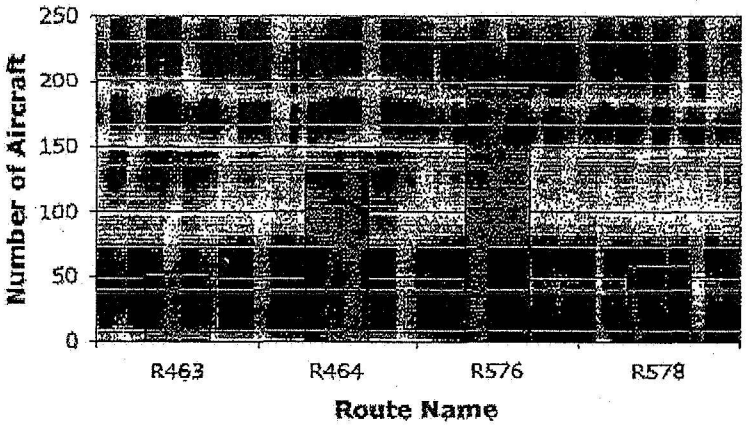

Figure 6. Westbound CEP Route Usage Statistics

IV. Modified Flow Characteristics

The results from an initial set of simulations that were designed to access the potential benefits and consequences of allowing flights to deviate from the fixed CEP route structure in favor of user-preferred routes are presented in this section. Using the ASDI data files for Dec. 14-16 and 19-20 of 2005, two sets of simulations were run in the Future ATM Concepts Evaluation Tool (FACET) [14]. In the first set of simulations, flights were allowed to fly along their filed flight plans, as specified in the ASDI files, while in the second set of simulations a wind optimal trajectory was calculated for each flight using the methodology outlined in Section II. For both sets of simulations, only aircraft that filed flight plans on one of the four westbound (i.e. R463, R464, R576, and R578) CEP routes were retained from the original ASDI files.

The magnitude and direction of the winds in the Pacific Ocean that were used to simulate the trajectory of the aircraft on both the original flight plan route and the wind optimal route were obtained from the Global Forecast System (GFS) Atmospheric Model [15] that is produced by the National Oceanic and Atmospheric Administration (NOAA). For reference, GFS is a global atmospheric model with a horizontal resolution of approximately 0.5^0 x 0.5^0 latitude/longitude and an unequally spaced vertical resolution starting at 1000 mb (surface) and extending up to 100 mb. Updates to the GFS model are available every six hours and forecasts are available up to 16 days into the future. As an example of the wind data used in the simulation, the wind magnitude contours at 250 mb, which roughly includes the altitudes between 31,000 ft and 36,000 ft, are shown in Fig. 7. For reference, the Hawaiian Islands are shown at the bottom left of this figure and the west coast of the United States is shown on the right side of this image. A region of very strong, easterly winds (>120 knots) is designated by the magenta polygon in the center of this figure and lies directly above two of the westbound CEP routes (R576 and R578).

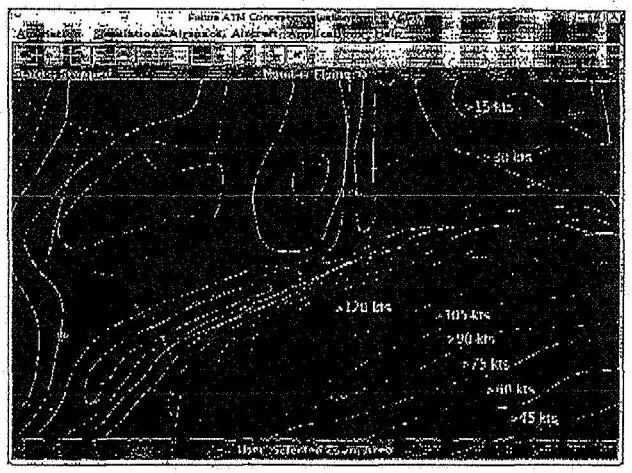

Figure 7. Wind contours at 250 mb in the Central East Pacific

The aircraft position (latitude and longitude) histories for the flight plan and wind optimal based simulations that were run using the ASDI data for Dec. 14, 2005 are displayed in Fig. 8. The leftmost image in this figure depicts the westbound position histories for aircraft on the CEP-based flight plan routes, and the rightmost image depicts the position histories for the flights on wind-optimal routes. Only minor deviations in the magnitude and direction of the wind-field were observed in the Central East Pacific on Dec. 14, 2005, so only a single GFS file (0:00 UTC, zero-hour forecast file) was used to generate these results. The most striking feature differentiating these two images is the tremendous latitudinal and longitudinal dispersion of the aircraft position histories resulting from the wind-optimal routing simulation. Not only are the histories dispersed but, with only one exception, the routes have all been shifted north because of the strong easterly winds present in Sector 3, see Fig. 8. When generating the wind optimal routes, each aircraft has been allowed to fly a wind optimal trajectory from the origin airport to the destination airport. *Alternative wind optimal strategies to be explored in the final draft of this paper include the following:*

1. *Fixed routing in the ARTCC airspace and wind optimal routing only in the oceanic environment*
2. *Wind optimal routing along a fixed number (e.g. 2-3) of dynamically generated routes*

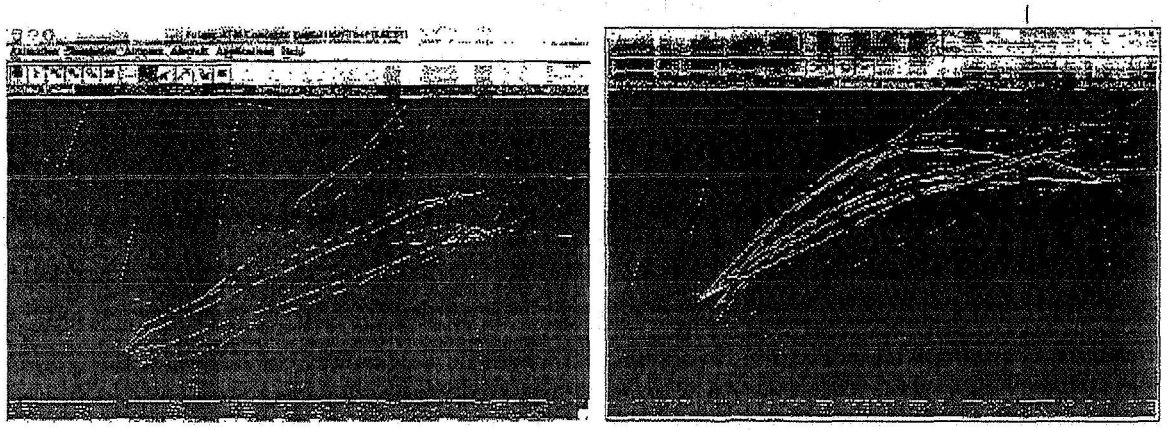

Figure 8. Flight Plan and Wind Optimal Routes for Westbound Flights

The sector counts as a function of time for Oakland Oceanic Sectors 3 and 4 are shown in Fig. 9 for both the CEP-based and wind-optimal routing simulations. The thick red and blue curves in this figure correspond to the CEP-based routing simulations, while the thin red and blue curves correspond to the wind optimal routing simulation. As can be seen from this figure, the impact of transitioning to wind optimal routes results in a decrease in the peak aircraft count in Sector 3 from eleven to one, and an increase in the peak aircraft count in Sector 4 from 18 to 27. From a controller workload perspective, the 50% increase in the peak traffic count in Sector 4 is a bit disconcerting. To accommodate the changes in the traffic patterns that could potentially be associated with adopting user preferred trajectories, resource scheduling algorithms [16] or dynamic re-sectorization [17] may prove beneficial. Both these areas of work will be explored in more detail in future studies.

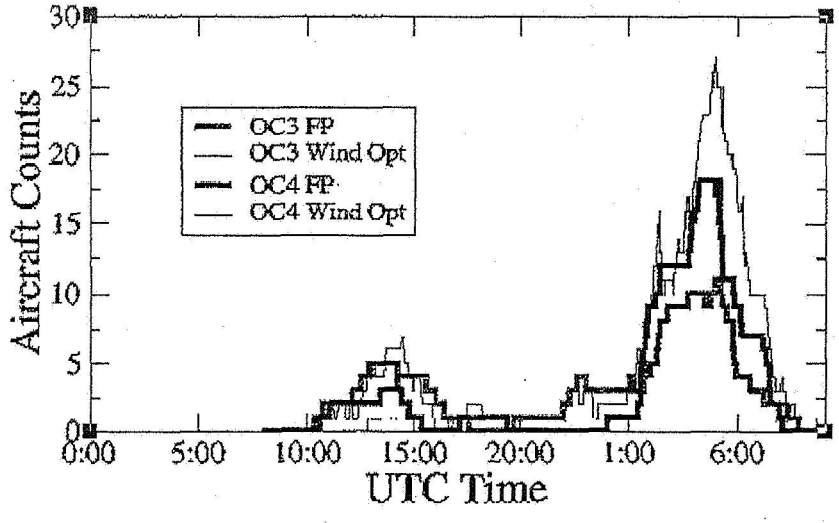

Figure 9. Aircraft Counts in Oakland Sectors 3 and 4 with wind optimal and CEP routing

Changes in the traffic patterns in the Central East Pacific can not only increase the workload of a controller, but also can give rise to an increase in the number of possible losses of separation. Using FACET, the simulated trajectories for all westbound flights were examined for possible losses of separation on both the nominal CEP-based flight plan routes and the wind-optimal routes. Losses of separation were identified under two different separation criteria: (1) 30 nmi lateral spacing, 30 nmi longitudinal spacing, and 1000 ft vertical spacing and (2) 50

nmi lateral spacing, 50 nmi longitudinal spacing and 1000 ft vertical spacing. For the remainder of this section, the first of these two separation standards will be referred to the "30/30" separation standard and the later of these two will be referred to as the "50/50" separation standard. Both of these separation standards are technically less restrictive than the standards that currently exist for flights on the CEP routes, though the 50/50 separation standards are achievable with the current ATOP system and the 30/30 separation standards are proposed reductions in the separation standards [2]-[3]. The geographical location of each unique, first-loss-of-separation event is depicted in Fig. 10. The leftmost image in this figure depicts these events with the 30/30 separation standards, while the rightmost image depicts these events with the 50/50 separation standards. Red circles are used to denote the CEP-based routing first-loss-of-separation events and blue squares are used for the wind-optimal events. Under both separation scenarios, the wind-optimal routing changes the location and frequency of the potential first-loss-of-separation events. The most striking feature to note regarding the location of the events is the large number of events that occur immediately upon entering the Oakland Oceanic Center. This would seem to indicate that additional departure constraints are required for each flight to ensure that the separation standards are met prior to passing control of flights from the domestic Centers to Oakland Oceanic. In addition, more first-loss-of-separation events are observed in Oakland Oceanic Sectors 4 and 7 under the wind-optimal routing scenario than the CEP-based routing scenario. This behavior is to be expected given the lack of structure and the numerous converging flight paths that are observed in Fig. 8 for the flights on wind-optimal routes.

In regards to the frequency of first-loss-of-separation events, the 30/30 scenarios yielded five events under the CEP-based routing simulation and four events for the wind-optimal routing simulation. As would be expected, the number of first-loss-of-separation events increased under the 50/50 scenario, yielding six events for the CEP-based routing simulation and 12 events for the wind-optimal routing simulation.

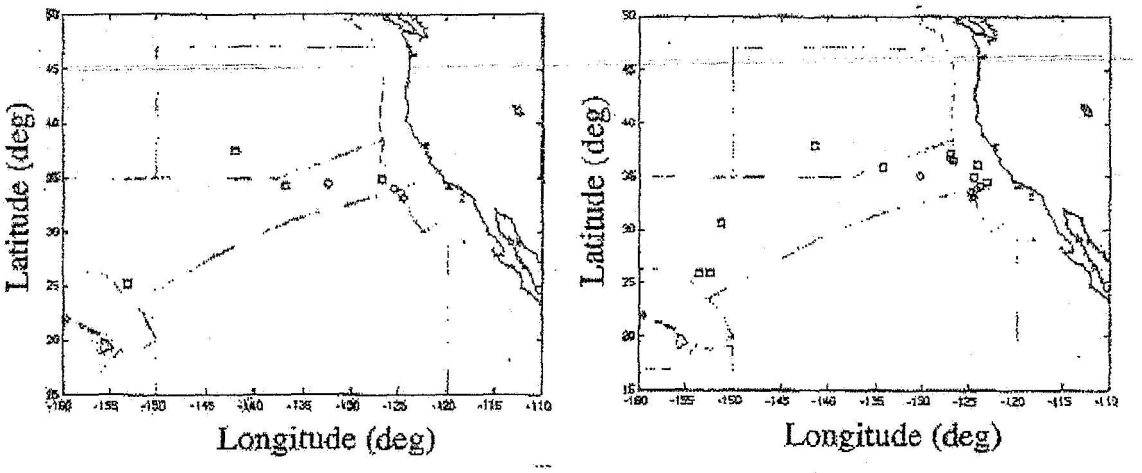

Figure 10. First-Loss-of-Separation Locations for Wind Optimal and CEP routing using 30/30 (left) and 50/50 (right) latitudinal/longitudinal separation standards

In the final draft of this manuscript, the sector count and first loss of separation analyses conducted for the westbound flights on Dec. 14, 2005 will be expanded to include the traffic from Dec. 15, 16, 19, and 20. In addition, the eastbound flights will also be examined. Additional metrics to be examined in the final draft include changes in travel time and distance.

V. Conclusion

With the introduction of the FAA's new ATOP system at Oakland Center, increased route flexibility and reduced separation standards can potentially now be accommodated. The results of an initial study that were designed to (1) understand the characteristics of traffic on the westbound CEP routes and (2) to assess the feasibility of transitioning from the CEP routes to user-preferred ones were presented. To accomplish the first of these two tasks, the ASDI data for Dec. 14-16 and 19-20 was used to examine the following: origin and destination of flights on the CEP

routes, usage of each route, vertical distribution of traffic on all routes, and the temporal distribution of flights on the routes.

As a surrogate for the user-preferred routes, a dynamic programming based methodology was presented and used to calculate wind optimal trajectories for the westbound flights that originally flew on CEP routes. The sector counts for Oakland Oceanic Sectors 3 and 4 and the location of the simulated first loss of separation events were compared for flights on both the wind optimal routes and the nominal CEP-based flight plan routes. Though the lateral and longitudinal distribution of flights was observed to change dramatically with the wind optimal routing the number of first-loss-of-separation events was not observed to change significantly.

Appendix A

For the current study, the cost associated with transitioning from an initial state, x_k, to a final state, x_{k+1}, is equal to the travel time between these two states. If the initial latitude/longitude position is denoted by (λ_i, τ_i) and the final position is denoted by (λ_f, τ_f) then the cost/travel time is given by [18]

$$C(x_k, u_k, k) = t = d / V_g \tag{X}$$

where

$$d = R_{earth} \cdot \cos^{-1}\left[\sin\lambda_i \cdot \sin\lambda_f + \cos(\tau_f - \tau_i) \cdot \cos\lambda_i \cdot \cos\lambda_f\right] \tag{X}$$

and

$$V_g = \sqrt{\dot{x}^2 + \dot{y}^2} \tag{X}$$

Here R_{earth} is the radius of the Earth, which is taken to be 3,444.046647 nm, and the horizontal components of the velocity are denoted by $\dot{x}$ and $\dot{y}$. These velocity components are calculated from the horizontal velocity of the aircraft, v_h, the horizontal component of the wind velocity, w_h, the aircraft's commanded heading, χ_{com}, and the horizontal wind direction, χ_h, using the following expressions:

$$\dot{x} = v_h \cdot \cos\chi_{com} + w_h \cdot \cos\chi_h \tag{X}$$

and

$$\dot{y} = v_h \cdot \sin\chi_{com} - w_h \cdot \sin\chi_h \tag{X}$$

The aircraft's command heading, χ_{com}, is related the course angle for great circle navigation via the following expression:

$$\chi_{com} = \chi_{GC} - \sin^{-1}\left(\left(w_h / v_h\right) \cdot \sin(\chi_h - \chi_{GC})\right) \tag{X}$$

where

$$\chi_{GC} = \tan^{-1}\left[\frac{\sin(\tau_f - \tau_i) \cdot \cos\lambda_f}{\sin\lambda_f \cdot \cos\lambda_i - \sin\lambda_i \cdot \cos\lambda_f \cdot \cos(\lambda_f - \lambda_i)}\right] \tag{X}$$

Acknowledgments

The authors would like to acknowledge the help of Mr. Kevin Chamness and Mr. David M. Maynard from the Federal Aviation Administration for providing the oceanic domain knowledge expertise required to complete this study. The assistance of Mrs. Almira Williams from CSSC, Inc. is also acknowledged for contributing to our understanding of flight routing and air traffic procedures in the Pacific Ocean.

References

[1]Wu, Y. S., Karakis, T., and Merkle, M., "Performance Metrics for Oceanic Air Traffic Management," *Air Traffic Control Quarterly*, Vol. 12, No. 4, 2004, pp. 315-338.

[2]"Air Traffic Control," Order 7110.65P, Federal Aviation Administration, Feb. 19, 2004.

[3]"Advanced Technologies & Oceanic Procedures (ATOP)", U.S. Dept. of Transportation, Federal Aviation Administration, URL: http://www.faa.gov/airports_airtraffic/technology/atop

[4]Trotter-Cox, A., "Required Navigation Performance (RNP)," *Professional Pilot Magazine*, 1999: URL: http://www.aviationmanuals.com/articles/article3.html.

[5]"Notice of Required Navigation Performance 10 (RNP-10) Implementation in the Oakland Center FIR," Oakland NOTAM A4335/98, Federal Aviation Administration, 1998.

[6]Erzberger, H. and Lee, H., "Constrained Optimum Trajectories with Specified Range," *AIAA Journal of Guidance, Navigation and Control*, Vol. 3, Jan-Feb, 1980, pp. 78-85.

[7]Jardin, M., "Real-Time Conflict Free Trajectory Optimization," *5th USA/Europe ATM 2003 R&D Seminar*, Budapest, Hungary, June 23-27, 2003.

[8]Bertsimas, D. and Patterson, S. S., "The Traffic Flow Management Rerouting Problem in Air Traffic Control: A Dynamic Network Flow Approach," *Transportation Science*, Vol. 34, No. 3, August 2000.

[9]Barnhart, C., Boland, N. L., Clarke, L. W., Johnson, G. L., Nemhauser, and G. L., Shenoi, R. G., "Flight String Models for Aircraft Fleeting and Routing," *Transportation Sciences*, Vol. 32, Issue 3, March 1998.

[10]Jardin, M., "Toward Real-Time En Route Air Traffic Control Optimization," Ph.D. Dissertation, Stanford University, Dept. of Aeronautics & Astronautics, April 2003.

[11]Larson, R. E. and Casti, J. L., *Principles of Dynamic Programming: Part 1 Basic Analytic and Computational Methods*, Marcel Dekker, Inc., 1978.

[12]"Enhanced Traffic Management System (ETMS)," Report No. VNTSC-DTS56-TMS-002, Volpe National Transportation Center, U.S. Dept. of Transportation, Cambridge, MA, Oct. 2005.

[13]"Aircraft Situation Display To Industry: Functional Description and Interface Control Document," Report No. ASDI-FD-001, Volpe National Transportation Center, U.S. Dept. of Transportation, Cambridge, MA, June 29, 2005.

[14]Bilimoria, K., Sridhar, B., Chatterji, G. B., Sheth, K., and Grabbe, S., "FACET: Future ATM Concepts Evalution Tool," *Air Traffic Control Quarterly*, Vol. 9, No. 1, 2001, pp. 1-20.

[15]"EMC Model Documentation," National Centers for Environmental Predictions, National Oceanic and Atmospheric Administration, URL: http://www.emc.ncep.noaa.gov/modelinfo/.

[16]Bertsimas, D., and Patterson S. S., "The Air Traffic Flow Management Problem with Enroute Capacities," *Operations Research*, Vol. 46, No. 3, May-June 1998, pp. 406-422.

[17]Sridhar, B., Sheth, K. S., Grabbe, S., "Airspace Complex and its Application in Air Traffic Management," *2nd USA/Europe Air Traffic Management R&D Seminar*, Orlando, FL, Dec. 1-4, 1998.

[18]Chatterji, G. B., Sridhar, B., and Bilimoria, K. D., "En-route Trajectory Prediction for Conflict Avoidance and Traffic Management," *AIAA Guidance Navigation and Control Conference*, San Diego, CA, July 29-31, 1996.